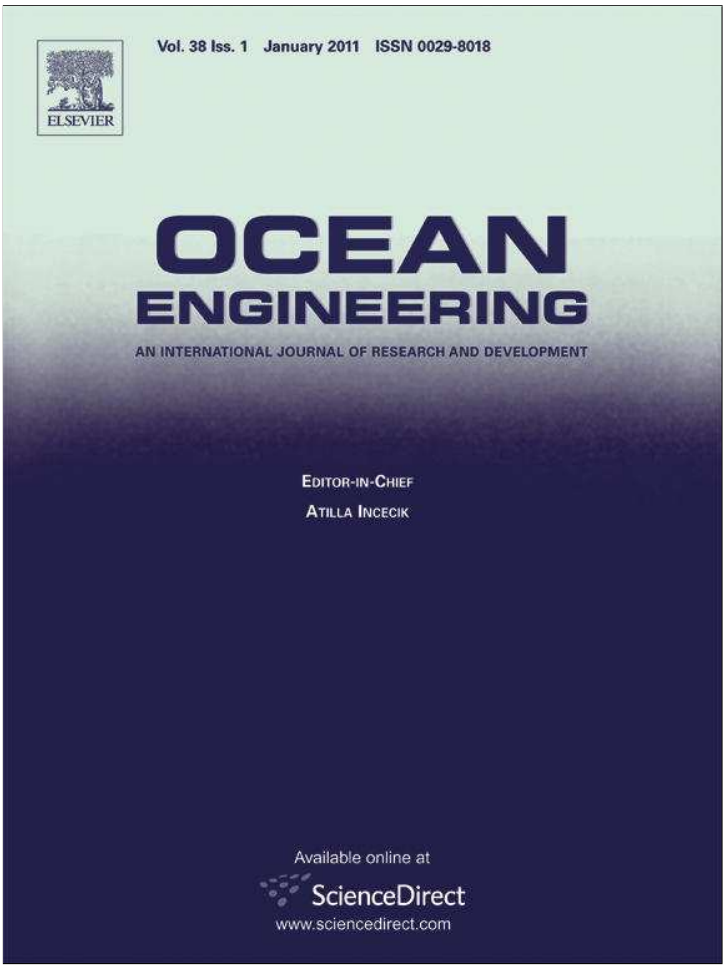

(This is a sample cover image for this issue. The actual cover is not yet available at this time.)

Ocean Engineering 42 (2012) 26–34

Contents lists available at SciVerse ScienceDirect

Ocean Engineering

journal homepage: www.elsevier.com/locate/oceaneng

Influence of grid type and turbulence model on the numerical prediction of the flow around marine propellers working in uniform inflow

Mitja Morgut*, Enrico Nobile

Dipartimento di Ingegneria Meccanica e Navale, University of Trieste, Trieste, Italy

ARTICLE INFO

Article history:
Received 21 July 2010
Accepted 2 January 2012
Editor-in-Chief: A.I. Incecik

Keywords:
RANS
Propeller
Grid typology
Turbulence modelling

ABSTRACT

In this work we analyze the influence of grid type and turbulence model on the numerical prediction of the flow around marine propellers, working in uniform inflow. The study is carried out comparing hexa-structured meshes with hybrid-unstructured meshes using the SST (Shear Stress Transport) turbulence model and the BSL-RSM (Baseline-Reynolds Stress Model) turbulence model. The simulations are carried out with a commercial CFD solver. The numerical results are compared with the available experimental data of two propellers in model scale. The comparison is carried out evaluating the global field values, represented by the thrust and torque coefficients, and also considering some local field values measured in the propeller wake. The computational results suggest that, for the numerical predictions of the propeller open water propulsion characteristics, the hexa-structured and hybrid-unstructured meshes can guarantee similar levels of accuracy. Nevertheless hybrid-unstructured meshes seem to exhibit a more diffusive character than hexa-structured meshes, and thus they are less suited for detailed investigations of the flow field. Finally, the two different turbulence models behave similarly on both types of meshes, with the BSL-RSM turbulence model providing only slightly better predictions than the computationally more economical SST turbulence model.

1. Introduction

Today both potential and viscous flow CFD (Computational Fluid Dynamics) codes are extensively used for design purposes, allowing experimental tests to be performed only in the final stages of the project. With reference to marine applications, CFD simulations can be used to predict the flow around hulls, appendages, and propellers.

For the case of the flow around a marine propeller, the numerical predictions have been first carried out using solvers based on the Lifting-Surface-Theory (Kerwin and Lee, 1978; Streckwall, 1986). The viscous RANS (Reynolds Averaged Navier Stokes) approach, on the other hand, was applied later (Kim and Stern, 1990). Subsequently, due to the progress of CFD technology and the continuous increase of computer performances, RANS solvers have become even more versatile and popular (Abdel-Maksoud et al., 1998; Oh and Kang, 1992; Chen and Stern, 1999; Stanier, 1999; Watanabe et al., 2003; Kawamura et al., 2006). Nevertheless, a successful RANS simulation is still influenced today by a lot of factors such as CAD geometry, topology and the dimension of the computational domain, meshing strategy, physical modelling. Regarding the meshing strategy, generally speaking, simulations carried out with hybrid-unstructured meshes i.e. – tetrahedral with prisms or hexahedral layers on solid surfaces – are less accurate than simulations carried out with hexahedral-structured grids. On the other hand, the generation of hybrid-unstructured meshes generally requires less effort than that needed to generate hexa-structured meshes. As a matter of fact, hybrid mesh generation is semi-automatic, while structured mesh generation is, in general, not automatic (as for as the decomposition of the domain in blocks is concerned), and consequently requires a significant amount of work.

Thus, in this work we investigated, mainly for the prediction of the propulsive characteristics rather than for a detailed investigation of the flow field, if the hexa-structured meshes can guarantee such better performances in terms of accuracy, convergence and computational time than hybrid-unstructured meshes, to justify the greater effort required for their generation. Furthermore on both typologies of mesh we also compared the SST (Shear Stress Transport) turbulence model with the BSL-RSM (Baseline-Reynolds Stress Model) turbulence model. The study was carried out on two propellers in model scale: the five-bladed propeller P5168 and the four-bladed propeller E779A. Numerical results were compared with the available experimental data.

Even though the present study was carried out mainly to give useful indications regarding the influence of the mesh typology

* Corresponding author. Tel.: +39 040 558 3502.
E-mail address: mmorgut@units.it (M. Morgut).

0029-8018/$ - see front matter © 2012 Elsevier Ltd. All rights reserved.
doi:10.1016/j.oceaneng.2012.01.012

on the numerical predictions of propeller performances, besides the global field values represented by the thrust, *Kt*, and torque, *Kq* coefficients, also some selected local field values were considered in order to enforce the reliability of the comparison.

With respect to the local flow analysis, in the case of the propeller P5168 we compared the circumferentially averaged velocity components, the contours of the root mean squares of the turbulent velocity fluctuations and the contours of the axial velocity component in the tip vortex region, evaluated in a plane downstream of the propeller's mid plane. For the case of propeller E779A we compared the local velocity profiles, evaluated in propeller's wake.

The numerical predictions of the propellers' open water characteristics carried out respectively with hexa-structured and hybrid-unstructured meshes guaranteed similar levels of accuracy, required a similar number of iterations to converge and therefore demanded similar computational times. However, comparing the local field values, hybrid-unstructured meshes were found to be significantly more diffusive than hexa-structured meshes. Therefore it seems that in order to capture the local flow characteristics with a similar level of accuracy the hybrid-unstructured meshes require a much finer spatial resolution than hexa-structured meshes. The two different turbulence models behave similarly on both types of mesh. Furthermore for the present study, in general terms, the computationally more expensive BSL-RSM turbulence model guaranteed only slightly better predictions than the computationally more economical SST turbulence model.

There follows a brief description of the propeller models and of the numerical method. Then a detailed description of the meshing strategies is presented, followed by the numerical results obtained first on propeller P5168 and then on propeller E779A. Finally, our concluding remarks are reported.

2. Propeller models

In this study two propellers in model scale, which are extensively used for the validation of CFD codes, were considered: propeller E779A, belonging to INSEAN, and propeller P5168 designed at the David Taylor Model Basin (DTMB). E779A is a four-bladed, fixed-pitch, low-skew propeller, designed in 1959 with a diameter of $D=0.227$ m. Since 1997 this propeller has been used in experimental activities performed by INSEAN aimed at providing a thorough characterization of marine propeller hydrodynamics and hydroacoustics over a wide range of operational conditions. P5168 is a five-bladed, controllable-pitch, highly skewed propeller with a diameter of $D=0.4027$ m. This propeller is mainly known for its experimental investigations, which are aimed at measuring tip-vortex cavitation inception, and near-tip velocity distribution in uniform inflow. The experimental measurements, considered in this paper, for propeller E779A were carried out in the towing tank and in the CEIMM cavitation tunnel (INSEAN, 2006), while for propeller P5168, the measurements were taken at the David Taylor 36-inch Variable Pressure Water Tunnel (Chesnakas and Jessup, 1998). In Fig. 1 the shapes of both propellers are shown.

3. Numerical strategy

The numerical predictions presented in this work were carried out with the ANSYS-CFX 11 (which will be referred from now on as CFX) commercial CFD solver. It employs the node-centered finite volume method (more precisely the Control Volume-Based Finite Element Method—CVFEM) (Schneider and Raw, 1987a,b). Moreover, it uses a coupled solver, accelerated by an Algebric Multigrid, to solve the hydrodynamic equations (for u, v, w, p) as a single system, with a fully implicit discretization of the equations at any given timestep (ANSYS, 2006a).

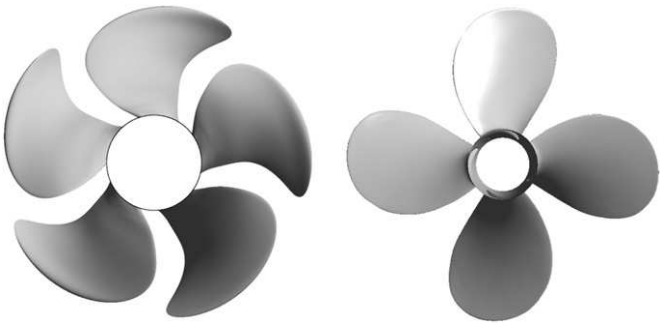

Fig. 1. Propeller shapes, P5168 (left), E779A (right). View looking downstream.

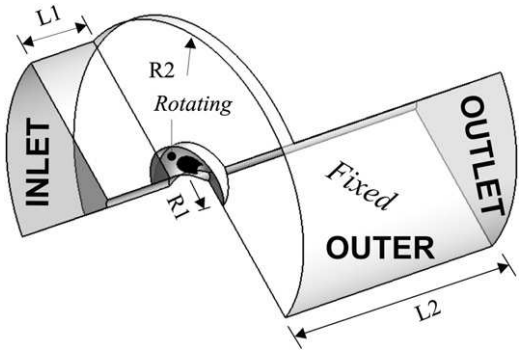

Fig. 2. Computational domain.

Table 1
Dimensions of the computational domains.

Values	P5168		E779A	
	Rotating	Fixed	Rotating	Fixed
R1	0.72D		0.70D	
Lmid	0.75D		0.76D	
R2		5D		5D
L1		3D		3D
L2		5D		5D

The MFR (Multiple Frame of Reference) approach was used to numerically predict the flow around the marine propeller. Since the flow around a marine propeller working in a homogeneous-uniform flow is periodic – with respect to the blades – numerical predictions were performed considering only one blade passage. The domain was thus defined, as illustrated in Fig. 2, by a segment of cylinder, covering only one blade, and was moreover subdivided into a rotating part, called *Rotating* and into a stationary part, called *Fixed*. The dimensions of the domains of both propellers are given in Table 1. In Table 1 the variable Lmid, not visible in Fig. 2, is the axial length of the *Rotating* part, and *D* is the propeller diameter. The inlet, outlet and outer boundaries of the *Fixed* part were placed far enough from the propeller in order to not affect the results. The distances were set through a domain independence study, carried out considering more shapes of the *Fixed* part, defined varying systematically L1, L2, R2. Finally the following boundary conditions were set. On the inlet boundary the turbulence intensity of 1% and a free stream velocity components were set. On the outlet boundary 0 Pa static pressure was imposed. On the periodic boundaries (sides of the domain) the rotational periodicity was ensured. On all solid surfaces the no

slip boundary condition was applied, and on the radial outer boundary the slip condition was imposed.

For turbulence closure, the SST and the BSL-RSM (for brevity RSM) turbulence models were used, both available in ANSYS-CFX, in combination with the automatic wall treatment.

In all calculations the High Resolution advective scheme (ANSYS, 2006a) was adopted.

4. Meshing

The influence of the grid type was investigated only in the region close to the propeller, i.e. the *Rotating* domain. This choice is due to the fact that for *Fixed*, because of the particular shapes of domain, using the hexa-structured approach, the decomposition of the domain in blocks led to highly distorted elements in the twisted region – over the *Rotating* – close to the outer boundary. For this reason we preferred to use the same hybrid-unstructured meshes for *Fixed*. This approach, after some preliminary studies, proved to guarantee the mesh independence for this part of the domain.

For the *Rotating* domain, as can be seen in Tables 2 and 3, three hexa-structured and three hybrid-unstructured meshes with different resolution levels were generated. The ANSYS-CFX 11 solver used in the present study, as previously noted, employs the CVFEM method. This implies that, to congruently compare different mesh types, the number of nodes, rather than the number of cells, should be matched.

For this reason, as can be seen from Tables 2 and 3, for *Rotating*, hexa-structured and hybrid-unstructured meshes of similar resolution level were generated, with a similar number of nodes and similar node distribution on the blade surface on hub surface and in the boundary layer region. As an example, Fig. 3 shows mid-resolution blade surface meshes of propeller P5168. All the meshes were generated using the ANSYS-ICEM CFD 11 commercial meshing tool. The hexa-structured meshes were generated analogously, as was done by other authors (for example Abdel-Maksoud et al., 1998; Berchiche and Janson, 2008), decomposing the *Rotating* part in a large number of blocks. The resolution and also the quality of the cells were set through a proper node distribution on the edges of the blocks.

Hybrid meshes were, instead, generated as follows. First, surface and volume tetrahedral meshes were generated using the robust OCTREE model (ANSYS, 2006b). Then, in order to

Table 2
Grids for the propeller P5168.

Grid	Nodes at rotating		Nodes at fixed
	Hexa	Hybrid	Hybrid
Coarse	259 632	258 899	116 339
Mid	554 820	536 985	116 339
Fine	1 197 252	1 118 045	116 339

Table 3
Grids for the propeller E779A.

Grid	Nodes at rotating		Nodes at fixed
	Hexa	Hybrid	Hybrid
Coarse	307 397	306 607	163 041
Mid	644 655	650 214	163 041
Fine	1 346 040	1 376 848	163 041

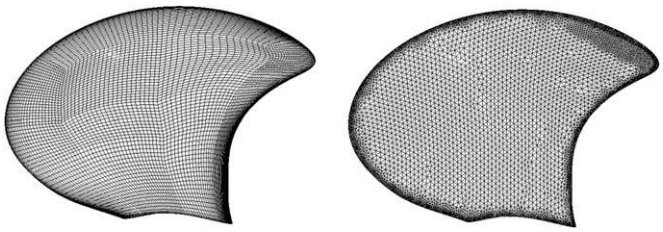

Fig. 3. Propeller P5168, surface meshes; hexa (left), hybrid (right).

Table 4
Setup for the propeller P5168.

J	N (RPM)	V (m/s)
0.98	1200	7.89
1.10	1450	10.70
1.27	1300	11.08
1.51	1150	11.73

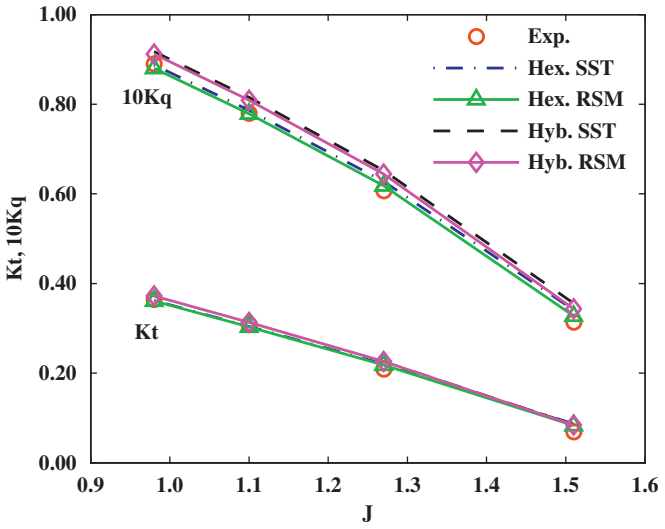

Fig. 4. Propeller P5168, characteristic curves computed using mid resolution meshes and both turbulence models.

Table 5
Propeller P5168: computational results with different mesh resolution levels and with the SST turbulence model.

J	Hexa						Hybrid					
	ΔKt (%)			ΔKq (%)			ΔKt (%)			ΔKq (%)		
	Coarse	Mid	Fine	Coarse	Mid	Fine	Coarse	Mid	Fine	Coarse	Mid	Fine
0.98	−0.9	−0.7	−0.3	0.4	−0.3	0.0	1.8	1.8	2.0	3.4	3.0	3.1
1.10	−1.1	−1.2	−0.7	1.8	0.9	1.3	1.4	1.6	1.9	4.5	4.5	4.6
1.27	5.0	4.9	5.4	4.6	3.4	3.7	7.0	8.1	8.5	6.8	7.4	7.6
1.51	14.6	25.9	27.4	8.3	8.5	9.0	14.6	25.3	26.6	9.2	13.2	13.7

resolve the turbulent boundary layer with a resolution similar to that of hexa-structured meshes, for both propellers 11 layers of prisms were placed around the hub and blade surfaces.

Moreover, for both propellers and for both typologies of meshes during the successive grid refinements, the distance of the first node from the solid surfaces, and consequently the average value of y^+, were kept unchanged. The average value of y^+ on solid surfaces (hub, blade), at design conditions, was 38 for propeller P5168 and 35 for propeller E779A, with y^+ defined as $y^+ = \mu_\tau y/\nu$ where $\mu_\tau = (\tau_w/\rho)^{1/2}$ is the friction velocity, y the normal distance from the wall, ν the kinematic viscosity, ρ the density and τ_w is the wall shear stress.

Table 6
Propeller P5168, mid resolution meshes: influence of turbulence modelling.

J	Hexa				Hybrid			
	ΔKt (%)		ΔKq (%)		ΔKt (%)		ΔKq (%)	
	SST	RSM	SST	RSM	SST	RSM	SST	RSM
0.98	−0.7	−1.0	−0.3	−1.1	1.8	1.9	3.0	2.5
1.10	−1.2	−1.7	0.9	−0.1	1.6	1.6	4.5	3.7
1.27	4.9	3.8	3.4	1.8	8.1	7.8	7.4	6.1
1.51	25.9	20.1	8.5	4.1	25.3	21.7	13.2	9.2

5. Results and discussion

To verify the influence of the grid type and of the turbulence modelling on the quality of predictions of the flow around a marine propeller, the numerical results were compared with the available experimental data.

For both propellers, the comparison was carried out between the global quantities, represented by thrust coefficient Kt and torque coefficient Kq, and also comparing a selection of local field values, computed in a plane located downstream of the propeller mid plane.

The thrust and torque coefficients were defined as follows:

$$Kt = \frac{T}{\rho n^2 D^4} \tag{1}$$

$$Kq = \frac{Q}{\rho n^2 D^5} \tag{2}$$

where T (N) is the thrust, Q (N m) the torque, n (rps) the rotational speed of a given propeller, D (m) the diameter of the propeller, and ρ (kg/m^3) is the density of the fluid.

Moreover, the relative percentage errors ΔKt and ΔKq listed in the next tables were defined as

$$\Delta Kt(\%) = \frac{Kt_{CFD} - Kt_{EXP}}{Kt_{EXP}} \cdot 100 \tag{3}$$

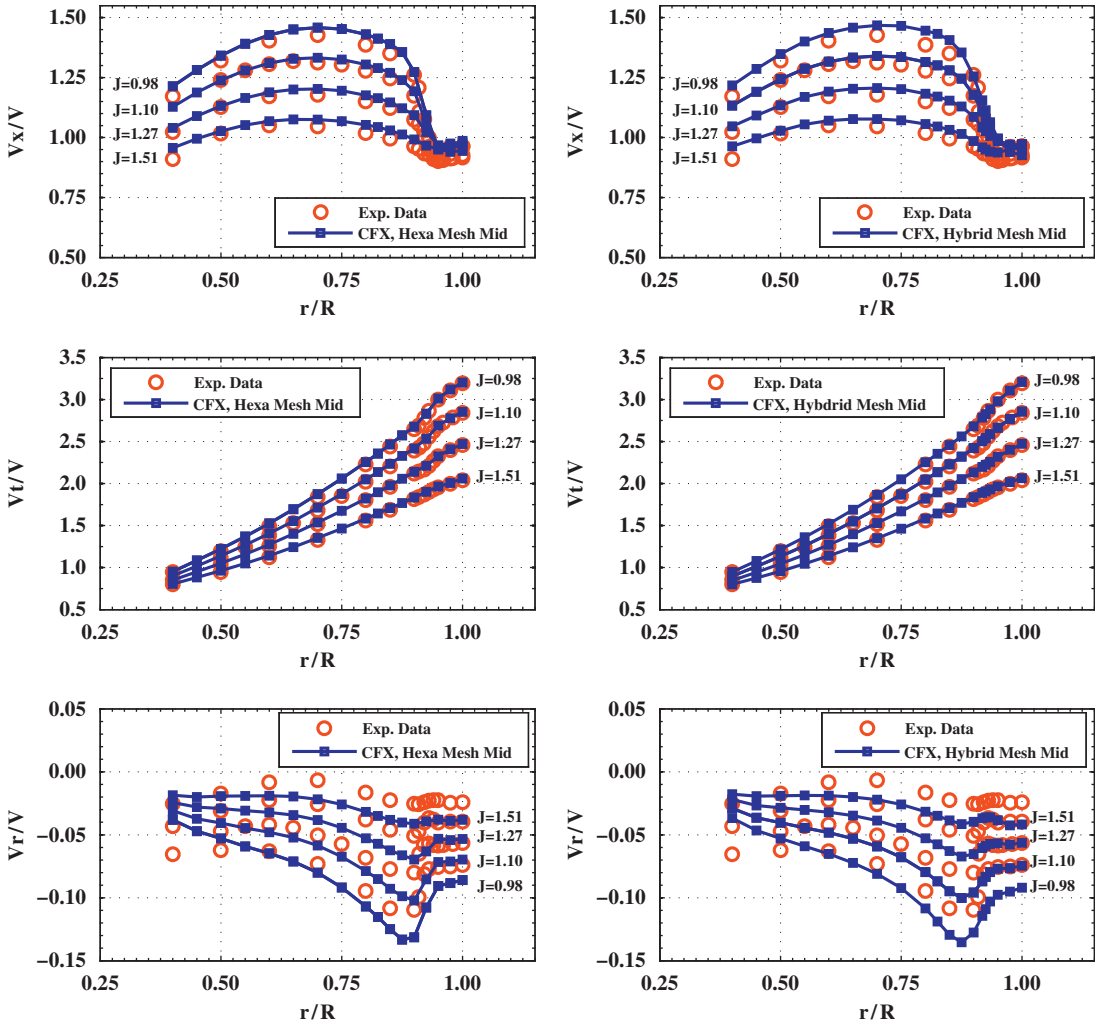

Fig. 5. Propeller P5168, circumferencially averaged velocity profiles computed using the RSM turbulence model at x/R=0.2386; hexa mesh (left), hybrid mesh (right).

$$\Delta Kq(\%) = \frac{Kq_{CFD} - Kq_{EXP}}{Kq_{EXP}} \cdot 100 \quad (4)$$

In the following sections, the study on propeller P5168 is presented first, followed by the investigation carried out on propeller E779A.

5.1. Propeller P5168

In the case of propeller P5168, the simulations were performed following the experimental setup (Chesnakas and Jessup, 1998) shown in Table 4, where N (rpm) is the rotational speed of the propeller, V (m/s) the velocity of the uniform free–stream flow and $J=V/nD$ the advance coefficient, with $n=N/60$. The flow upstream of the propeller was assumed uniform, even though during the experimental measurements, a wake from three upstream shaft support struts was present. In this study we used a water with density $\rho = 997$ kg/m^3 and with a dynamic viscosity $\mu = 8.89 \times 10^{-4}$ kg/m s. The Reynolds number was defined as $Re_{0.7R} = C_{0.7R}V_{0.7R}/\nu$, where $C_{0.7R}$ was the propeller blade chord at 70% of radius R, and $V_{0.7R}$ was the total velocity incoming to blade section at 70% of radius, defined as $V_{0.7R} = \sqrt{V^2+(2\pi n 0.7R)^2}$. Thus, the simulations carried out at the four different advance coefficients, $J=0.98$, 1.10, 1.27, 1.51, corresponded to the four different Reynolds numbers $Re_{0.7R}=(3.81, 4.70, 4.35, 4.05)\times 10^6$. For propeller P5168 the study of the influence of the grid resolution was carried out considering all four different operational points investigated experimentally by Chesnakas and Jessup (1998). The results in Table 5 are collected as obtained on the hexa-structured and hybrid-unstructured meshes of different resolution levels in combination with the SST turbulence model. From the values of the relative percentage errors it is possible to note that grid resolution had a similar effect on both grid typologies for the prediction of the global quantities. In fact, for both meshing approaches, the predicted values of Kt and Kq on the meshes with mid resolution were very close to those on the meshes with fine resolution.

In the following the results obtained on the mid-resolution meshes in combination with the SST turbulence model as well as with the BSL-RSM are discussed.

Regarding the propulsive performances, from the characteristic curves depicted in Fig. 4 and values collected in Table 6 it is clear that the hexa-structured mesh and hybrid-unstructured mesh provided similar trends, with both relative errors on Kt and Kq growing with the increment of the advance coefficient (J). In general terms the predictions carried out with the BSL-RSM turbulence model were slightly more accurate than those carried out with the SST turbulence model.

As far as the local flow field analysis is concerned following the study of Rhee and Joshi (2005), the averaged velocity components and the root mean square (RMS) of the turbulent velocity fluctuations, q, were evaluated in the plane $x/R=0.2386$ downstream of the propeller mid plane, where x is the axial distance and R is the radius of the propeller. The root mean square (RMS) of the turbulent velocity fluctuations, q, was defined as $q=\sqrt{2k}$, where k is the turbulent kinetic energy.

From Fig. 5 it is visible how the circumferentially averaged axial (Vx), tangential (Vt), and radial (Vr) velocity components predicted with both grids were very similar to each other, for the different operational conditions, J, and at various radial distances, r. The radial distance, r, is intended from the propeller's rotational axis centerline. Further, it is interesting to note that the axial and tangential velocity components were very close to the experimental data, while the radial components were not so close. However it has to be kept in mind, that for the radial components, the values are lower and, consequently, we expect that also the experimental uncertainty is larger.

The contours of q/V presented in Fig. 6 compared qualitatively well with the experimental data. However, quantitatively the magnitude of the predicted turbulent velocity fluctuations did not agree well with the experimental data, in particular on the hybrid-unstructured mesh, where, as clearly visible in Fig. 6, the effect of the numerical diffusion was more pronounced.

In order to further highlight the different diffusive behaviour/character of the two different mesh typologies, we qualitatively

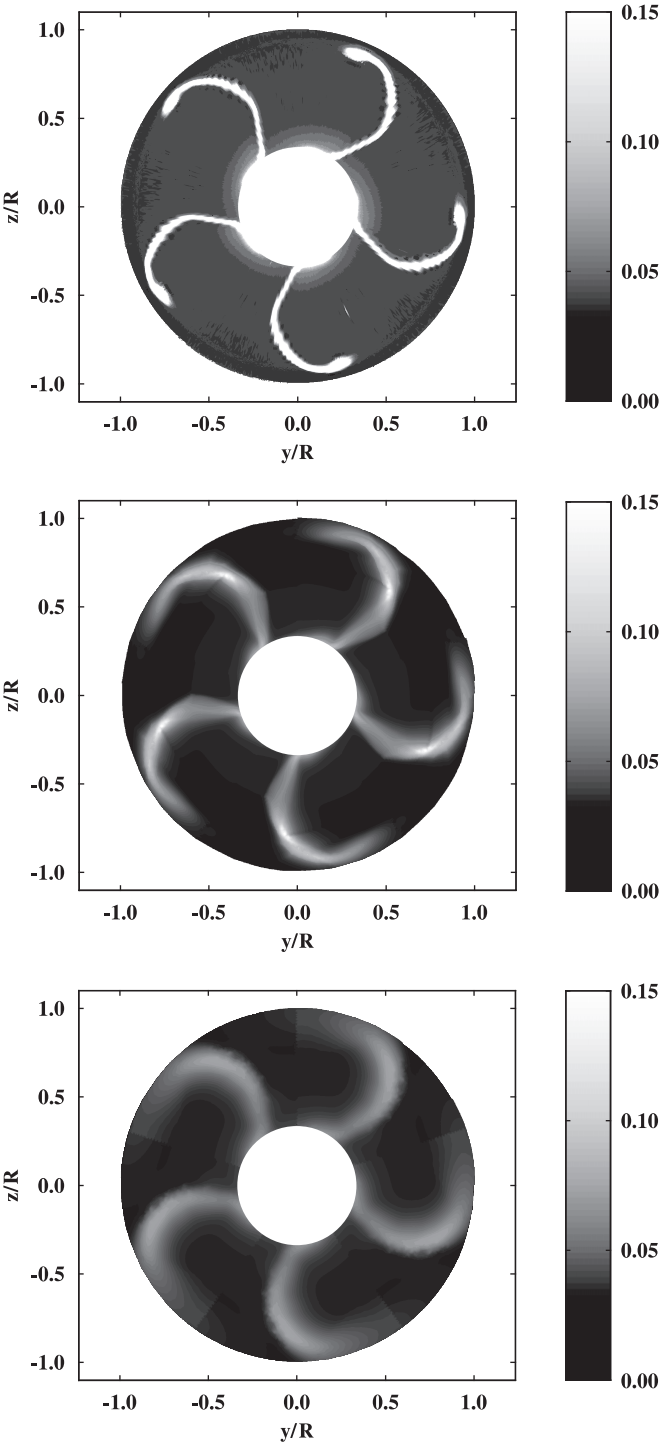

Fig. 6. Propeller P5168, q/V contours computed using mid resolution meshes and the RSM turbulence model in $x/R=0.2386$ plane for $J=1.1$; experimental (top), hexa (middle), hybrid (bottom).

analyzed the tip vortex core structure. In order to properly capture this detail we generated two additional meshes refined in the tip vortex core region, with 2.6×10^6 number of nodes, as suggested by Hsiao and Pauley (1999), Hsiao and Chahine (2008), and Qiu et al. (2009). The tip vortex flow, observed experimentally at $J=1.1$ in the plane $x/R=0.2386$, was numerically predicted using both turbulence models. In Fig. 7 the contours of the axial velocity field, Vx/V computed with the SST turbulence model are presented. In the same figure the experimental flow field was obtained by averaging the velocities from all five tip vortices. From these contours it is possible to appreciate the higher diffusivity of the hybrid-unstructured meshes. It is interesting to note that the flow field computed on the hexa-structured mid resolution mesh (Fig. 7b) was qualitatively similar to that of the much more finer hybrid-unstructured mesh with tip vortex core refinement (Fig. 7e).

As a matter of fact the best resolution corresponding to the hexa-structured mesh with the tip vortex core refinement (Fig. 7c) qualitatively compared well with the experimental data even though the position of the vortex did not perfectly match the experimental one.

It is important to add that, even though the finest meshes allowed better resolution of the tip-vortex flow region, in terms of the Kt and the Kq the predicted values differed less than 0.6% from those computed on the mid-resolution meshes for both turbulence models. The same trend was verified also for $J=1.27$.

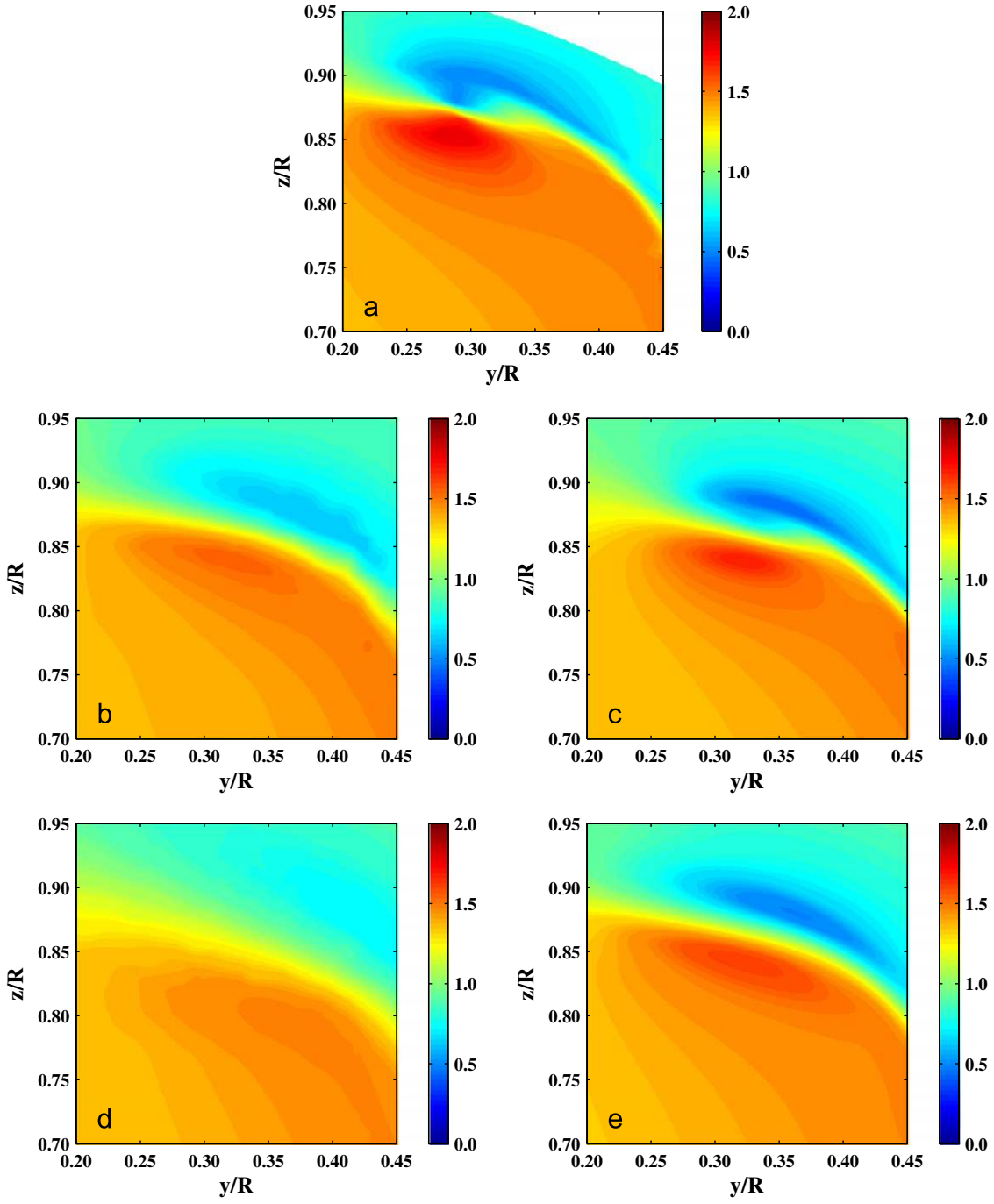

Fig. 7. Propeller P5168, contours of Vx/V in the tip vortex region computed with the SST turbulence model in $x/R=0.2386$ plane for $J=1.1$; (a) experimental, (b)hexa mid, (c) hexa with vortex refinement, (d) hybrid mid, (e) hybrid with vortex refinement.

Table 7
Propeller E779A: influence of the mesh resolution using the SST turbulence model.

J	Hexa						Hybrid					
	ΔKt (%)			ΔKq (%)			ΔKt (%)			ΔKq (%)		
	Coarse	Mid	Fine	Coarse	Mid	Fine	Coarse	Mid	Fine	Coarse	Mid	Fine
0.71	0.8	1.1	0.5	3.4	3.5	2.8	0.5	0.5	1.5	3.9	3.3	4.2
0.88	−2.5	−2.1	−2.7	2.2	2.3	1.7	−0.7	−1.8	0.2	5.4	3.4	5.4

In fact for this propeller the predictions of the propulsive performances were influenced principally by the mesh typology, while the turbulence models and the detailed resolution of the tip vortex flow played a secondary role.

Summarizing, from the overall result we did not notice marked differences between hexa-structured and hybrid-unstructured meshes for the prediction of the overall propeller performances. They predicted the values of Kt and Kq with similar levels of accuracy. Moreover, the simulations carried out at a given J required, on both grid types, the same number of iterations to push the flow field equation residuals very close to, or below, the convergence target set to 1.0×10^{-5}. Therefore the computational time of simulations carried out with meshes of different type but with the same resolution level was similar. Finally, on both mesh types the predictions of Kt and Kq were, in general terms, slightly more accurate in combination with the RSM turbulence model.

5.2. Propeller E779A

For propeller E779A, like propeller P5168, the study of the influence of the grid resolution was performed first. However, in this case, only two different operational points were considered, $J=0.88$ (design condition) and $J=0.71$ (Pereira et al., 2004). The grid-resolution study was carried out in accordance with the towing tank's experimental setup (INSEAN, 2006), using the SST turbulence model. From the results collected in Table 7 it can be seen that, for a given J, the predicted values on hexa-structured meshes with different resolution levels were very similar to each other. Vice versa, in the case of the hybrid approach, for a given J, the predicted values on meshes with different resolution levels were less homogeneous.

Since the objective of the present study was to compare different types of meshes for the prediction of propeller performances, we decided to perform the rest of the simulations with mid-resolution meshes, as a compromise between accuracy and computing times.

In Table 8 and Fig. 8 the results obtained with the two mesh types in combination with both turbulence models are presented. In this case the different operational conditions were set keeping fix the rotational speed of the propeller, and varying the inflow velocity. The Reynolds number was in the range of $4.6 \times 10^5 \leq Re_{0.7R} \leq 8.5 \times 10^5$. In general terms, the predictions carried out with the RSM turbulence model were slightly more accurate than those carried out with the SST turbulence model. Moreover, differently from propeller P5168, the thrust in general terms was, surprisingly, better predicted on the hybrid-unstructured mesh. However, the maximum difference between predicted values on different meshes was less than 3.0%.

Also for the propeller E779A the different meshing approaches were further compared, analogously to Greco et al. (2004) considering some selected local field values. In this case we considered the circumferential velocity components in axial and radial directions, taken for $J=0.88$ in the plane $x/R=0.2$ downstream of the propeller's mid plane. The experimental

Table 8
Propeller E779A: selected results.

J	Hexa				Hybrid			
	ΔKt (%)		ΔKq (%)		ΔKt (%)		ΔKq (%)	
	SST	RSM	SST	RSM	SST	RSM	SST	RSM
0.249	3.0	2.7	5.8	5.7	0.6	3.4	3.9	4.5
0.348	3.6	3.1	6.1	5.7	1.0	1.6	4.1	4.3
0.447	2.8	2.3	5.3	4.8	0.9	1.7	3.9	4.5
0.546	2.0	1.8	4.6	4.0	0.7	1.5	3.7	3.1
0.646	1.5	1.3	4.1	3.4	0.6	1.3	3.6	2.6
0.710	1.1	1.1	3.5	2.7	0.5	1.2	3.3	2.1
0.880	−2.1	−1.3	2.3	1.7	−1.8	−0.8	3.4	1.4
0.945	−2.2	−1.3	3.3	2.5	−1.9	−0.6	4.9	2.4
1.045	−0.7	0.2	5.0	3.9	−1.5	0.6	6.2	3.0

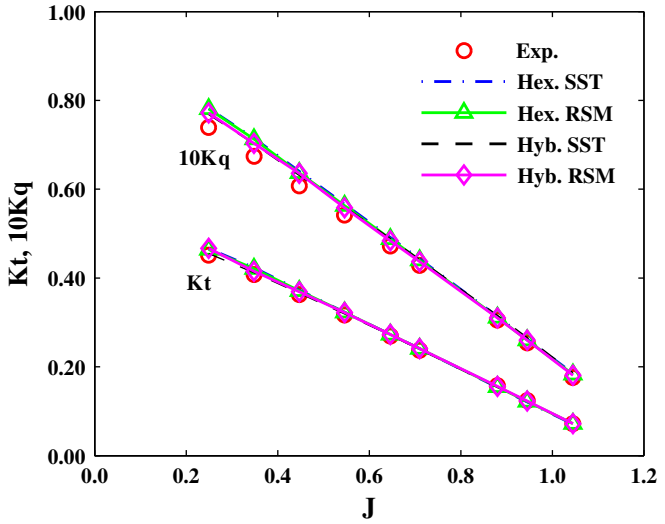

Fig. 8. Propeller E779A, characteristic curves computed using mid resolution meshes and the RSM turbulence model.

measurements of the local field values, at $J=0.88$, were taken in the cavitation tunnel. For this reason, in order to compare the numerical values with the experimental data in the most congruent manner, four additional numerical predictions were performed at $J=0.88$, following the cavitation tunnel experimental setup corresponding to a Reynolds number of the order of $Re_{0.7R} = 1.4 \times 10^6$. In what follows a selection of numerical results is presented. Figs. 9 and 10 show the axial and radial velocity profiles, computed on both types of mesh and using both turbulence models, in a plane $x/R=0.2$ downstream of the propeller's mid plane at $r/R=0.7$ and $r/R=0.9$, respectively. From Figs. 9 and 10 it can be seen that the velocity profiles, computed on different mesh types and using different turbulence models, were close to

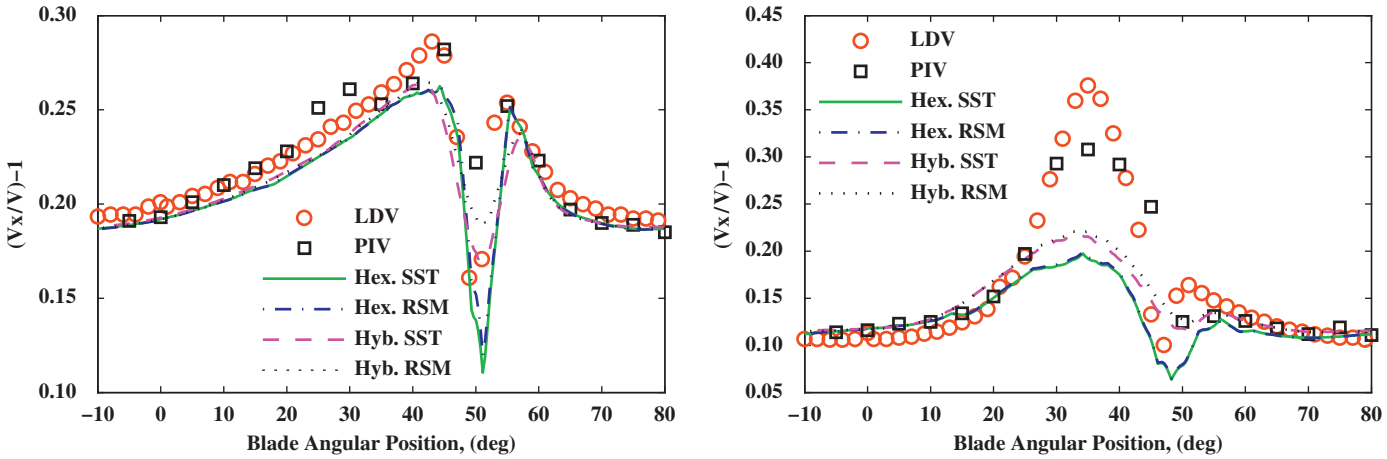

Fig. 9. Propeller E779A, axial velocity components computed on mid resolution meshes using the SST and the BSL-RSM turbulence models in $x/R=0.2$ plane and at $r/R=0.7$ (left), $r/R=0.9$ (right).

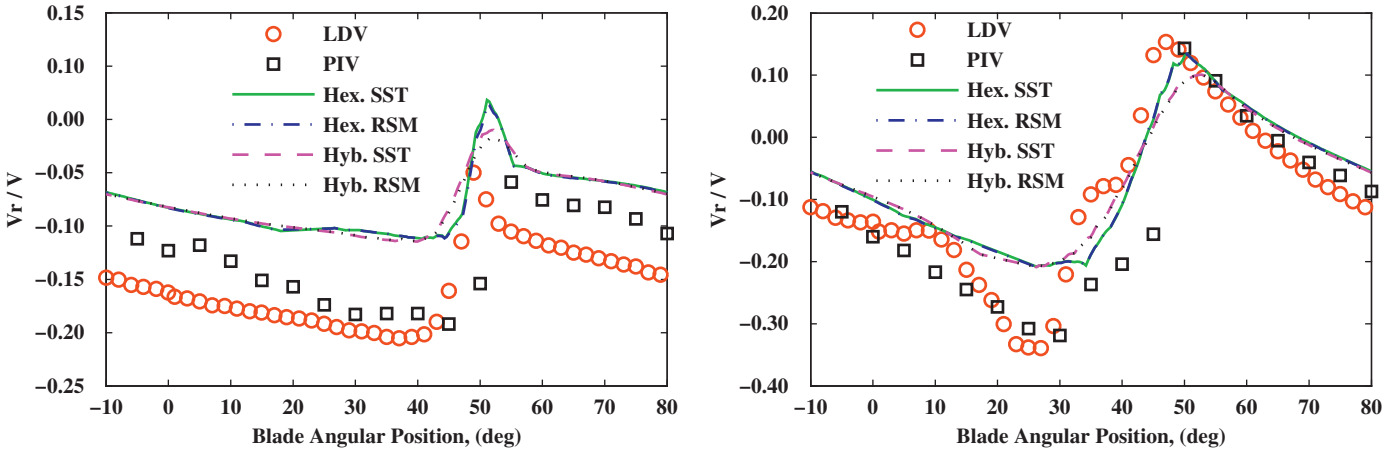

Fig. 10. Propeller E779A, radial velocity components computed on mid resolution meshes using the SST and the BSL-RSM turbulence models in $x/R=0.2$ plane at $r/R=0.7$ (left), $r/R=0.9$ (right).

each other, and qualitatively they compared well with the experimental data. However, quantitatively the numerical velocity profiles did not agree completely with the experimental data. In particular the peaks and hollows predicted on hybrid-unstructured mesh, due to the greater diffusion, were smoother than those predicted on the hexa-structured mesh.

Finally we mention that, also in this case, simulations carried out with different grid types and different turbulence models, exhibited similar convergence trends and therefore they required similar computing times.

6. Concluding remarks

Generally speaking, CFD simulations carried out on hexa-structured meshes provide results which are more accurate than those obtained on hybrid-unstructured meshes. However the hexa-structured meshes, compared to hybrid-unstructured ones, generally require more effort for their generation. Thus in this work we investigated, principally for the prediction of propeller open water characteristics, whether the hexa-structured meshes can guarantee significantly better performances, in terms of accuracy and computational time, than hybrid-unstructured meshes to justify the greater effort required for their generation. Furthermore, we also investigated to what extent the numerical predictions carried out on both typologies of mesh are influenced by RANS type turbulence modelling. In particular we compared the well known two-equation SST turbulence model with the BSL-RSM turbulence model. While the former may be nowadays considered as a workhorse for practical engineering calculations, the second is representative of a class of advanced turbulence models capable of tacking problems, like the flow around marine propellers, where anisotropy of the turbulent quantities may play a significant role. The investigations were carried out using two propellers in model scale: propeller E779A and propeller P5168, and comparing numerical results with the available experimental data. In particular, for both propellers the global field values, represented by the thrust and torque coefficients, and some selected local field values measured in the propeller wake were compared. The numerical results were obtained with ANSYS-CFX 11 for steady state conditions.

The overall results suggest that for the numerical predictions of the open water characteristics, with the present numerical method, the hexa-structured and hybrid-unstructured meshes can guarantee, with comparable computational times, similar levels of accuracy. However, the hybrid-unstructured meshes exhibit a more diffusive character than hexa-structured meshes, and therefore, for a detailed investigation of the local flow field, the latter is a better choice.

The two selected turbulence models influence the numerical predictions on both types of mesh in a similar manner. In general terms the computationally more expensive BSL-RSM turbulence

model seems to guarantee only slightly more accurate predictions than the computationally more economical SST turbulence model. Thus, for the numerical prediction of the propeller (open water) performances, the latter might be a more effective choice.

Acknowledgements

We wish to thank Prof. Eric Paterson, Pennsylvania State University, PA and INSEAN, in particular Dr. Francesco Salvatore, for providing us the geometry and the experimental measurements for propeller P5168 and E779A, respectively.

Partial financial support was provided by project *OpenSHIP*, Simulazioni di fluidodinamica computazionale (CFD) di alta qualità per le previsioni di prestazioni idrodinamiche del sistema carena elica in ambiente OpenSOURCE, supported by Regione FVG POR FESR 2007–2013 Obiettivo competitività regionale e occupazione.

References

Abdel-Maksoud, M., Menter, F., Wuttke, H., 1998. Viscous flow simulations for conventional and high-skew marine propellers. Schiffstechnik/Ship Technol. Res. 45, 64–71.

ANSYS, 2006a. ANSYS CFX Solver Theory Guide, Release 11.0.

ANSYS, 2006b. ANSYS ICEM CFD User Guide, Release 11.0.

Berchiche, N., Janson, C.-E., 2008. Grid influence on the propeller open-water performance and flow field. Schiffstechnik/Ship Technol. Res. 55, 87–96.

Chen, B., Stern, F., 1999. Computational fluid dynamics of four-quadrant marine-propulsor flow. J. Ship Res. 43 (4), 218–228.

Chesnakas, C., Jessup, S., 1998. Experimental characterization of propeller tip flow. In: Proceedings of the 22nd Symposium on Naval Hydrodynamics, Washington, DC, USA, pp. 156–170.

Greco, L., Salvatore, F., Di Felice, F., 2004. Validation of a quasi-potential flow model for the analysis of marine propellers wake. In: 25th Symposium on Naval Hydrodynamics. St. John's, Newfounland, Canada.

Hsiao, C.-T., Chahine, G.L., 2008. Scaling of tip vortex cavitation inception for a marine open propeller. In: 27th Symposium on Naval Hydrodynamics, Seoul, Korea.

Hsiao, C.-T., Pauley, L.L., 1999. Numerical computation of tip vortex flow generated by a marine propeller. J. Fluids Eng. 121, 638–645.

INSEAN, 2006. The INSEAN E779A Propeller Dataset. Technical Report. INSEAN, The Italian Ship Model Basin, Propulsion and Cavitation Laboratory.

Kawamura, T., Takekoshi, Y., Yamaguchi, H., Minowa, T., Maeda, M., Fujii, A., Kimura, K., Taketani, T., 2006. Simulation of unsteady cavitating flow around marine propeller using a RANS CFD code. In: 6th International Symposium on Cavitation (CAV2006), Wageningen, The Netherlands.

Kerwin, J.E., Lee, C.S., 1978. Prediction of steady and unsteady marine propeller performance by numerical lifting-surface theory. Trans. SNAME 86 (4), 218–253.

Kim, H.T., Stern, F., 1990. Viscous flow around a propeller-shaft configuration with infinite-pitch rectangular blades. J. Propul. 6, 434–443.

Oh, K.-J., Kang, S.-H., 1992. Numerical calculation of the viscous flow around a rotating marine propeller. KSME J. 6 (2), 140–148.

Pereira, F., Salvatore, F., Di Felice, F., 2004. Measurement and modeling of propeller cavitation in uniform inflow. J. Fluids Eng. 126, 671–679.

Qiu, W., Peng, H., Liu, L., Hsiao, C.T., 2009. A study of tip vortex flow of a marine propeller based on RANS solution. In: 16th International Conference of Ship and Shipping Research, Messina, Italy.

Rhee, S.H., Joshi, S., 2005. Computational Validation for Flow around a Marine Propeller Using Unstructured Mesh Based Navier-Stokes Solver. JSME International Journal, Series B 48 (3), 562–570.

Schneider, G., Raw, M., 1987a. Control volume finite-element method for heat transfer and fluid flow using colocated variables. 1. Computational procedure. Numer. Heat Transfer 11, 363–390.

Schneider, G., Raw, M., 1987b. Control volume finite-element method for heat transfer and fluid flow using colocated variables. 2. Application and validation. Numer. Heat Transfer 11, 391–400.

Stanier, M., 1999. The application of 'RANS' code to investigate propeller scale effects. In: 22nd Symposium on Naval Hydrodynamics, Washington, DC, USA.

Streckwall, H., 1986. A method to predict the extent of cavitation on marine propellers by lifting-surface-theory. In: International Symposium on Cavitation, Sendai, Japan.

Watanabe, T., Kawamura, T., Takekoshi, Y., Maeda, M., Rhee, S.H., 2003. Simulation of steady and unsteady cavitation on a marine propeller using a RANS CFD code. In: 5th International Symposium on Cavitation (CAV2003), Osaka, Japan.